Environmental Science & Technology

Article

Cite This: Environ. Sci. Technol. 2020, 54, 92−101

pubs.acs.org/est

Diesel Soot and Amine-Containing Organic Sulfate Aerosols in an Arctic Oil Field

Matthew J. Gunsch,[†,#] Jun Liu,[†,#] Claire E. Moffett,[§] Rebecca J. Sheesley,[§] Ningxin Wang,[∥] Qi Zhang,[∥] Thomas B. Watson,[⊥] and Kerri A. Pratt*[,†,‡]

[†]Department of Chemistry and [‡]Department of Earth and Environmental Sciences, University of Michigan, Ann Arbor, Michigan 48109, United States

[§]Department of Environmental Science, Baylor University, Waco, Texas 76798, United States

[∥]Department of Environmental Toxicology, University of California, Davis, California 95616, United States

[⊥]Department of Environmental and Climate Sciences, Brookhaven National Laboratory, Upton, New York 11973, United States

Supporting Information

ABSTRACT: The rapid decrease in Arctic sea ice is motivating development and increasing oil and gas extraction activities. However, few observations of these local Arctic emissions exist, limiting the understanding of impacts on atmospheric composition and climate. To address this knowledge gap, the chemical composition of atmospheric aerosols was measured within the North Slope of Alaska oil fields during August and September 2016 using an aerosol time-of-flight mass spectrometer (ATOFMS) and a time-of-flight aerosol chemical speciation monitor (ToF-ACSM). Plumes from oil and gas extraction activities were characterized by soot internally mixed with sulfate (matching diesel soot) and organic carbon particles containing aminium sulfate salts. Sea spray aerosol at the coastal site was frequently internally mixed with sulfate and nitrate, from multiphase chemical processing from elevated NO_x and SO_2 within the oil field. Background (nonplume) air masses were characterized by aged combustion aerosol. No periods of "clean" (nonpolluted) Arctic air were observed. The composition of the nonrefractory aerosol measured with the ACSM was similar during plume and background periods and was consistent with the mass concentrations of nonrefractory particles measured by ATOFMS. Two ultrafine aerosol growth events were observed during oil field background periods and were correlated with fine mode amine-containing particles.

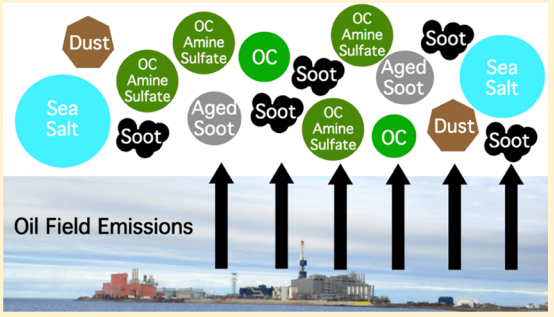

INTRODUCTION

The Arctic is now more accessible to oil exploration and development,[1,2] as surface temperatures are increasing at nearly twice the global average[3,4] and sea ice is rapidly declining.[5−7] An estimated 30% of the world's undiscovered gas and 13% of the undiscovered oil are located in the Arctic.[8] In 2016, Alaska sold new leases for over 2400 km^2 of land for oil and gas extraction on the North Slope of Alaska and in the Beaufort Sea; this was the second-largest sale since 1998.[9] Similar expansions are occurring elsewhere, particularly in Russia and Norway.[8]

Oil and gas extraction activities emit particulate matter (PM),[10,11] with negative effects on air quality and human health.[12] Atmospheric particles impact climate[4,10] by scattering or absorbing incoming solar radiation, acting as cloud condensation and ice nuclei, and altering snow albedo.[13] Arctic oil and gas extraction activities in 2004 are estimated to have emitted 15 kt black carbon (BC) and 16 kt organic carbon (OC), with total emissions of 47 kt of PM.[10] These activities also emitted 150 kt of SO_2, 160 kt of NO_x (NO + NO_2), and 120 kt of nonmethane volatile organic compounds.[10] These trace gases can oxidize in the atmosphere forming lower volatility compounds, which condense to form secondary aerosol.[12] Local Arctic BC sources are simulated to have a greater impact on Arctic climate than transported BC,[14−16] with recent assessments suggesting that BC is underpredicted by models by an average factor of 2.5 in the Arctic.[17] The prediction and global transportation of BC from various source regions have been improved in recent years.[18−20] However, large uncertainties still remain for inventories of local Arctic emissions.[21] Winiger et al.[20] examined PM carbon isotopes across five circum-Arctic sites and found that 61%, on average, of annual mean BC was from fossil fuel combustion, with the highest fossil fuel influence (85%) at Utqiaġvik (Barrow), Alaska.

There have only been a few studies that have examined emissions from Arctic oil and gas extraction activities.[22−29]

Received: August 9, 2019
Revised: November 15, 2019
Accepted: December 2, 2019
Published: December 16, 2019

DOI: 10.1021/acs.est.9b04825
Environ. Sci. Technol. 2020, 54, 92−101

Measurements in the Norwegian Arctic showed increased NO_x, SO_2, and BC in plumes originating from offshore extraction facilities.[26] Ground- and aircraft-based campaigns within and downwind of the North Slope of Alaska oil fields have shown elevated BC, NO_x, SO_2, CO_2, CH_4, and cloud condensation nuclei (CCN) concentrations.[22−24,29,30]

The distribution of chemical species across the aerosol population, or mixing state, determines individual particle properties, including optical properties (scattering/absorption), hygroscopicity, toxicity, and chemical reactivity.[12,31] Uncertainties in the BC mixing state have contributed to uncertainties in the estimations of BC climate impacts in the Arctic.[32] Single-particle mass spectrometry directly measures the chemical composition and mixing state of individual particles.[33] Unique, source-specific mass spectral signatures[34] are used to identify the source of each individual particle. Single-particle mass spectrometry can differentiate between gasoline, diesel, residual fuel, coal, and biomass combustion emissions.[35−42]

The sources, chemical composition, and mixing states of atmospheric aerosols from Arctic oil field emissions were investigated through measurements within the North Slope of Alaska (Prudhoe Bay) oil fields during August and September 2016 at Oliktok Point, Alaska. An aerosol time-of-flight mass spectrometer (ATOFMS) measured the size and chemical composition of individual particles[43] and a time-of-flight aerosol chemical speciation monitor (ToF-ACSM) measured the nonrefractory aerosol chemical composition.[44,45] The aerosol composition and concentrations within combustion plumes and regional oil field background air masses are compared.

EXPERIMENTAL SECTION

Field Site and Instrumentation. The field campaign was conducted from August 22 to September 17, 2016 at Oliktok Point, Alaska, at the Department of Energy (DOE) Atmospheric Radiation Measurement (ARM) Mobile Facility (AMF3) (70°29′41.4″ N, 149°53′10.9″ W). The surrounding oil fields are located both onshore and offshore and cover an area of over 14 000 km^2 of land and ocean (Figure 1, http://dog.dnr.alaska.gov). The Beaufort Sea is located ∼0.5 km to the north, northwest, and northeast and ∼1 km to the east of the site. Meteorological data, including wind speed, wind direction, relative humidity, and temperature, were collected with a Vaisala WXT520 weather transmitter at a height of ∼10 m.[46] Radiation data were obtained from the ARM Sky Radiometers on Stand for Downwelling Radiation (SKYRAD).[47] Carbon dioxide (CO_2) was measured by a cavity ringdown spectrometer (model G2301, Picarro) from a height of ∼10 m.[48]

A time-of-flight aerosol chemical speciation monitor (Tof-ACSM)[44,45] is part of the suite of instruments operated by the ARM program at Oliktok Point. The Tof-ACSM-measured speciated mass loadings averaged over 30 min. It has a mass resolution of $m/\Delta m$ = 600 and detection limits of ∼0.30 ng m^{-3} for a 30 min signal average. A collection efficiency of 0.5 was applied to the ACSM mass concentration.[44] Positive matrix factorization was performed for the ACSM organic aerosol (OA) mass spectra,[49−51] and two factors were identified: hydrocarbon-like OA (HOA) and oxygenated OA (OOA).[44,52]

An aerosol time-of-flight mass spectrometer (ATOFMS), described below, measured the size-resolved chemical composition of individual particles.[43] BC mass concentrations were measured online (5 min resolution) by a seven-wavelength aethalometer (model AE42, Magee Scientific) and corrected following the procedure described by Schmid et al.[53] Aerosol particle size distributions (13−746 nm mobility diameter, d_m, and 0.5−20 μm aerodynamic diameter, d_a) were measured using a scanning mobility particle sizer (SMPS, model 3082, TSI, Inc.) and an aerodynamic particle sizer (APS, model 3321, TSI, Inc.), respectively. Using the method of Khlystov et al.,[54] the SMPS and APS size distributions were combined into a continuous size distribution from 0.013 to 2.5 μm (d_a), assuming a shape factor of 1 and a density of 1.5 g cm^{-3}. The air sampled by these instruments was collected through an inlet at a height of 5.4 m through a PM_{10} Teflon-coated aluminum cyclone (URG Corporation) at a flow rate of 40 L min^{-1}. The flow was split with a stainless steel cylindrical manifold into foam-insulated copper sampling lines for each of the instruments.

Figure 1. Map of North Slope of Alaska oil fields and images of local emission sources near the AMF3 field site (yellow star). The map background was provided by ArcGIS 10.3.1 with the World Imagery basemap (sources: Esri, DigitalGlobe, GeoEye, Earthstar Geographics, CNES/Airbus DS, USDA, USGS, AeroGRID, IGN, and the GIS User Community). Oil field extent was obtained from http://dog.dnr.alaska.gov. Photo credit: Matthew Gunsch.

Single-Particle Mass Spectrometry. An aerosol time-of-flight mass spectrometer (ATOFMS), based on the design of Pratt et al.,[43] measured the size and chemical composition of 32 880 individual particles from 0.07 to 1.6 μm (vacuum aerodynamic diameter) in real time. Briefly, particles were focused through an aerodynamic lens system and entered the sizing region as a narrow, collimated beam. Particle diameter was calibrated using 0.09−2 μm polystyrene latex spheres (Polysciences, Inc.) with a density of 1 g cm^{-3}. Particle diameters were determined by measuring the time each particle took to traverse two continuous wave lasers (50 mW of 405 nm and 50 mW of 488 nm, Coherent Technol.). The particles then entered a dual-polarity reflectron time-of-flight mass spectrometer (Tofwerk) and were individually desorbed and ionized by a 266 nm Nd:YAG pulsed laser (Centurion, Quantel, Inc.), operating at 0.8−1.2 mJ, resulting in positive

DOI: 10.1021/acs.est.9b04825
Environ. Sci. Technol. 2020, 54, 92−101

and negative ion mass spectra. The sample stream and particles were dried in-line through two silica gel diffusion driers. Negative ion mass spectra were collected for only 63% of particles, by number, because of water accumulation that suppressed negative ion formation,[55] as commonly observed in other marine environments.[56]

Individual particle mass spectra were imported and analyzed in FATES, a custom single-particle mass spectrometer analysis toolkit for MATLAB (MathWorks).[57] Individual particle mass spectra were clustered based on the presence and intensity of ion peaks using an ART-2a neural network algorithm with a vigilance factor of 0.8 and a learning rate of 0.05 for 20 iterations.[58] The resulting clusters were grouped into eight unique groups, each representing an individual particle type, based on the most likely m/z assignments, according to ion ratios and spectral identification from previous studies.[34] Note that the individual particle mass spectra were grouped by ART-2a based on the overall similarity in ion presence and intensity, with the particle class names reflecting the majority composition; however, due to individual particle heterogeneity, some particles within a given particle type may not have every signature peak in the average mass spectra of that particle type.

Using the method of Qin et al.,[59] ATOFMS particle numbers were scaled using the SMPS and APS data to obtain chemically resolved number and mass concentrations. A set of effective densities were applied to convert from number to mass concentration based on previously reported composition-dependent densities[60−67] and a comparison of the ATOFMS and SMPS/APS size distributions: OC (1 g cm^{-3}), elemental carbon (EC) (1.3 g cm^{-3}), OC−amine−sulfate (1.5 g cm^{-3}), EC and OC (ECOC) (1.2 g cm^{-3}), incineration particles (1.8 g cm^{-3}), mineral dust (2 g cm^{-3}), biomass burning (1.4 g cm^{-3}), and sea spray aerosol (1.8 g cm^{-3}).

Radiocarbon. Total suspended particulate matter samples were collected on quartz fiber filters using a HI-Q high volume sampler (HVP-5300AFC; HI-Q Environmental Products Company, Inc.). Samples were collected for 4−7 days each at a flow rate of 1.2 m^3 min^{-1}. Analysis for OC and EC utilized the NIOSH 5040 method[68] and a thermal−optical transmittance carbon analyzer (Sunset Laboratories). EC harvested from the samples was analyzed for radiocarbon abundance at the Woods Hole National Oceanic Sciences Accelerator Mass Spectrometry facility; sample preparation and data analysis were performed following the method described by Yoon et al.[69]

RESULTS AND DISCUSSION

Single-Particle Chemical Characterization. Eight unique individual particle types were identified by ATOFMS for August 22−September 17, 2016. These were sea spray aerosol (SSA), EC, ECOC, OC−amine−sulfate, OC, biomass burning, mineral dust, and incineration particles (Figures 2, 3, and S1). The average contributions of biomass burning, mineral dust, and incineration particles were 8, 3, and 1%, respectively, of the 0.07−1.6 μm particle number concentrations. This analysis focuses on the most abundant particle types: EC, ECOC, OC−amine−sulfate, OC, and SSA. Mass spectra of the minor particle types are described in the Supporting Information.

Single-particle SSA mass spectra were characterized by positive ion peaks at m/z 23 (Na^+) and 81, 83 (Na_2Cl^+), as well as negative ion peaks at m/z −35, −37 (Cl^-), and −93, −95 ($NaCl_2^-$).[70] SSA was primarily observed at diameters

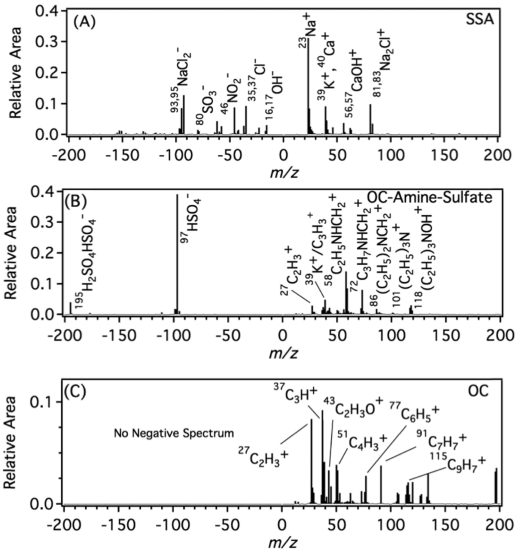

Figure 2. Average individual particle ATOFMS mass spectra for major particle types observed: (A) sea spray aerosol (SSA), (B) organic carbon (OC)−amine−sulfate, and (C) OC.

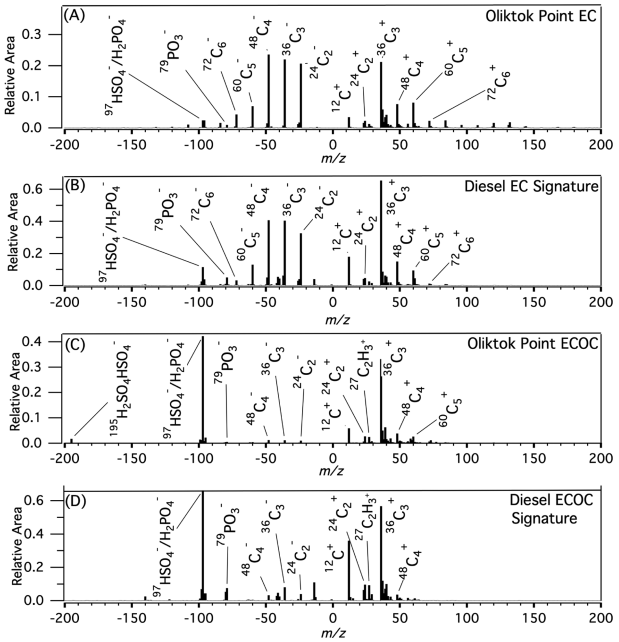

Figure 3. Average individual particle ATOFMS EC (A) and ECOC (C) mass spectra observed at Oliktok Point, compared to diesel combustion EC (B) and ECOC (D) ATOFMS mass spectral signatures from source studies by Toner et al.[37]

above 0.6 μm but with some particles as small as 0.2 μm (Figure S5). These observations are consistent with previous summertime measurements in the Alaskan Arctic.[27,71]

Individual OC particles were identified by peaks at m/z 27 ($C_2H_3^+$), 37 (C_3H^+), and 43 ($C_2H_3O^+$), from both hydrocarbon and oxidized (secondary) OC compounds.[60,72,73] Additional peaks at m/z 51 ($C_4H_3^+$), 77 ($C_6H_5^+$), 91 ($C_7H_7^+$), and 115 ($C_9H_7^+$) are consistent with aromatic hydrocarbons and suggestive of a combustion source.[36,73] Negative ion mass spectra were not observed for these OC particles because of ion suppression from water accumulation.[55] These OC particles were present across both

DOI: 10.1021/acs.est.9b04825
Environ. Sci. Technol. 2020, 54, 92−101

submicron and supermicron size ranges (Figure S5), consistent with aged particles that had accumulated secondary material during atmospheric transport.

OC−amine−sulfate particles were characterized by OC (e.g., m/z 27, $C_2H_3^+$) and sulfate (m/z −97, HSO_4^-) ion markers, as well as unique contributions from diethylamine (DEA, m/z 58, 72, $C_2H_5NHCH_2^+$, $C_3H_7NHCH_2^+$), trimethylamine (TMA, m/z 59, $N(CH_3)_3^+$), triethylamine (TEA, m/z 86, 101, $(C_2H_5)_2NCH_2^+$, $(C_2H_5)_3N^+$), and triethylamine-oxide (TEAO, m/z 118, $(C_2H_5)_3NOH^+$) (Figure 2).[74] Average number and mass fractions of OC−amine−sulfate particles through the study were 34 and 32%, respectively. Internally mixed amine and sulfate particles are consistent with the presence of nonvolatile aminium sulfate salts,[75] particularly given the minimal ammonium (m/z 18, NH_4^+), which was only observed in 23% of the OC−amine−sulfate particles. The OC−amine−sulfate particle mass spectra also included sulfuric acid (m/z −195, $H_2SO_4HSO_4^-$), indicative of particle acidity[75,76] and required for the formation of aminium sulfate salts.[75,77] The particles had intense peaks corresponding to ethylamines. Diethylamine and triethylamine are typically associated with anthropogenic sources, including vehicular combustion and industrial processes.[74,78,79] Nearby onshore well drilling, oil extraction, pipeline operation, gas-fired turbines and heaters, flares, gas processing facilities, seawater treatment facilities, wastewater treatment facilities, and mobile vehicular emissions are all possible sources, which may have contributed to the amine-containing particles observed. In addition, there was influence from marine biogenic amines, including TMA, which has been observed in aerosols in the Canadian Archipelago,[80,81] as well as Antarctica.[82,83] Recent work in the Antarctic shows a marine source of DEA contributing to aerosols.[82] As discussed below, the OC−amine−sulfate particles were most abundant during oil field plumes, suggesting that these particles were primarily anthropogenic in origin.

EC (soot) particle mass spectra featured both positive and negative carbon cluster ions ($C_n^{+/-}$), along with phosphate at m/z −79 (PO_3^-) (Figure 3).[31,37,84] ECOC particles were identified by carbon cluster ions ($C_n^{+/-}$), OC (m/z 27, $C_2H_3^+$),[85] oxidized OC (m/z 43, $C_2H_3O^+$),[60] sulfate (m/z −97, HSO_4^-), and sulfuric acid (m/z −195, $H_2SO_4HSO_4^-$). The average EC and ECOC mass spectra were compared to ATOFMS mass spectra from combustion source studies, following the method described by Toner et al.,[37] by calculating the dot products between the ambient and source mass spectra to quantify their similarity. A higher dot product indicates greater similarity between the ambient and source particle mass spectra, whereas a lower dot product indicates less similarity.[34,76] The mass spectra of EC and ECOC showed a high degree of similarity with those of the top two diesel particle types,[37] with dot products of 0.94 and 0.93 for EC and ECOC, respectively (Figure 3). Notably, the presence of phosphate in the EC particle mass spectra is because of phosphate-based additives in lubricating oils used in diesel engines.[72] These diesel soot particles are consistent with the prevalence of diesel combustion in the oil fields. Comparing carbonaceous particle types to mass spectra from gasoline-powered combustion[37] resulted in dot products less than 0.75, further confirming the minimal influence of gasoline combustion within the oil fields. Previous carbon isotope measurements show a small gas flaring contribution to BC on the North Slope of Alaska,[20] suggesting only minor contribution to the observed EC and ECOC.

The ACSM measured the nonrefractory mass concentrations of OA, sulfate, nitrate, and ammonium in PM_1 (Figure 5). These species were internally mixed within the OC, OC−amine−sulfate, ECOC, and biomass burning particles, measured by ATOFMS (Figure 2). The sum of the mass concentrations of the primarily nonrefractory particles measured by ATOFMS (OC−amine−sulfate, OC, and biomass burning particles) was correlated with (R = 0.66, Figure S6), and higher by an average of 31% than, the sum of the nonrefractory mass measured by the ACSM. Note that this 31% difference is in line with the ∼30% uncertainty of the instruments.[86,87] A small mass fraction of the biomass burning particles consisted of refractory salts, including potassium sulfate,[88] contributing to the high bias. The larger particle size range of 0.07−1.6 μm of the ATOFMS, compared to 0.04−1 μm for ACSM, also contributed to the lower ACSM-measured mass loadings. The remaining 37% of the ATOFMS-measured mass, on average, consisted of refractory SSA, EC, mineral dust, and incineration particles, as expected for the coastal oil field site.

Oil Field Plume Characterization. Oil and gas extraction emissions impact the Oliktok field site all of the time and from all directions (Figure 1). The site was frequently in plumes, characterized by BC mass concentrations greater than 0.2 μg m^{-3}, as measured by the aethalometer, and CO_2 mole ratios greater than 397 ppm. Both BC and CO_2, at these levels, are indicative of combustion within the oil fields.[22,23] The site was in combustion plumes 29% of the time between August 22 and September 17, 2016 and in background air masses the remainder of the time (Figure 5), as discussed in the following section.

Elevated $PM_{2.5}$ number and mass concentrations of 1400 particles cm^{-3} and 2.6 μg m^{-3}, on average, were observed within plume periods, based on SMPS and APS measurements. These events primarily consisted of sub-100 nm particles with the average particle number mode of 50 nm (Figure S2), indicating the presence of fresh combustion emissions.[89] A Kolmogorov−Smirnov goodness-of-fit statistical test shows that above 200 nm the aerosol number distributions during plume and oil field background air mass periods were statistically similar (σ = 0.05). This indicates that the plumes are primarily adding trace gas precursors and ultrafine particles to the background aerosol distribution.

During the study, 15 682 individual particles ranging from 0.07 to 1.6 μm were chemically characterized by ATOFMS within direct plumes (Figure S5). When the maximum number concentrations were observed on August 27 and 28, ∼80% of the 0.07−1.6 μm particles, by number, corresponded to EC and ECOC (Figure 5). This was a relatively stagnant period with low winds of 3 m s^{-1} (Figure S3) when diesel-fueled heavy machinery moved an oil rig on a road located ∼1 km to the east of the site.

The particle number concentrations within plumes were dominated by carbonaceous particles, including 36% EC, 11% ECOC, 5% OC, and 23% OC−amine−sulfate particles (Figures 4 and 5). EC particles were primarily less than 200 nm and accounted for 40%, by number, of the 70−200 nm particles during both plume and oil field background periods (Figure S5). OC−amine−sulfate particles were primarily detected with diameters less than 700 nm and contributed ∼60%, by number, between 300 and 500 nm (Figure S5).

DOI: 10.1021/acs.est.9b04825
Environ. Sci. Technol. 2020, 54, 92−101

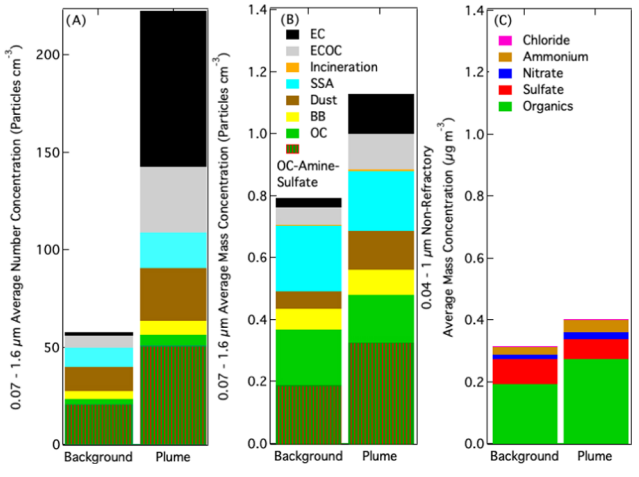

Figure 4. Chemically resolved average (A) number and (B) mass concentrations for 0.07−1.6 μm particles, measured by ATOFMS, and (C) mass concentrations of nonrefractory species measured by ACSM within 0.04−1 μm particles, during oil field background and direct plume air mass influence periods at Oliktok Point, AK.

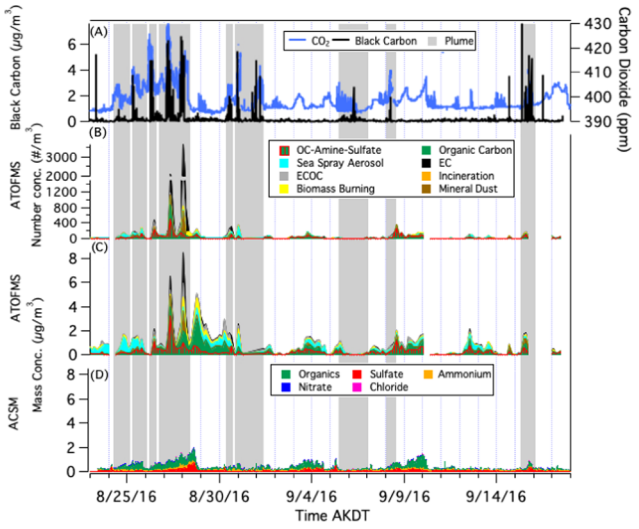

Figure 5. (A) Black carbon (BC) mass concentrations and CO_2 mole ratios; a 3 h time resolution chemically resolved (B) number and (C) mass concentrations, based on ATOFMS measurements (0.07−1.6 μm); and (D) 0.5 h time resolution nonrefractory species mass concentrations by ACSM within 0.04−1 μm particles.

Sulfate was internally mixed within 97% of ECOC and 91% of OC−amine−sulfate particles, by number. Only 29% of the EC particles, by number, contained sulfate. The average mass concentrations of 0.13 μg m^{-3} EC, 0.11 μg m^{-3} ECOC, and 0.33 μg m^{-3} OC−amine−sulfate particles were observed and elevated compared to that during background periods (Figure 4). Consistent with the combustion influence, the average HOA mass concentration, as measured by the ACSM, was 0.15 μg m^{-3} within the plumes and was ∼20% higher than the 0.12 μg m^{-3} OOA (Figure S7). $PM_{2.5}$ BC mass concentrations measured by the aethalometer averaged 0.43 μg m^{-3} during plumes, with brief, extreme spikes up to a maximum of 7.6 μg m^{-3} on August 28.

Measurements of filter-based EC concentrations and radiocarbon apportionment were completed for the plume period of August 24−28 (Figure 5) and a similarly high EC period at the end of the study from September 18 to 21, 2016. The EC concentrations were 0.19 ± 0.02 and 0.24 ± 0.03 μg m^{-3} for the August and September periods, respectively. The EC fraction corresponding to fossil fuel, rather than modern carbon (e.g., biomass burning), was 81 ± 8% for the August period and 90 ± 12% for the September period, further confirming that the EC was dominated by local fossil sources during plume periods. Note that the filter-based EC concentrations were lower than BC during plume periods, primarily due to the different time resolution of the measurements (4−7 day filter samples vs 5 min resolution).

Even during plumes, SSA accounted for ∼20% of the observed mass at an average of 0.22 μg m^{-3} and contributed ∼40%, by number, to the 0.8−1.6 μm particles (Figures 4 and S5) because the ocean was approximately 0.5 km away. During the plume periods, the average number fractions of SSA particles containing nitrate and sulfate were 77 and 40%, respectively. To investigate differences in SSA composition between the plume and background periods, the average dual-polarity SSA mass spectrum during plumes was subtracted from the average spectrum during background periods (Figure S8). The SSA particles in the plumes had increased intensities in sodium nitrate (m/z −131, $NaNO_2NO_3^-$ and −147, $Na(NO_3)_2^-$) and sodium sulfate (m/z −119, $NaSO_4^-$ and +165, $Na_3SO_4^+$); increased intensities in nitrate (m/z −46, NO_2^-, and −62, NO_3^-) and sulfate (m/z −80, SO_2^-) and decreased intensities in chloride (m/z −35, −37, Cl^-), were also observed. Note that m/z −80 is used to identify sulfate due to an interference with $NaCl_2^-$ at m/z −97.[60] The internal mixing of sulfate and nitrate with SSA is evidence of multiphase processing within the combustion plumes.[90,91]

Oil Field Background Aerosol Characterization. When direct plumes were not observed at the site, the winds were typically from the prevailing north/northeast and represented oil field background air mass conditions (Figure S3). Average $PM_{2.5}$ number and concentrations were 307 particles cm^{-3} and 1.2 μg m^{-3}, respectively, with a particle number mode of 105 nm (Figures S2 and S4). These background concentrations are higher than those observed during August−September at other Arctic locations, including Station Nord, Greenland (227 particles cm^{-3}),[92] Tiksi, Russia (222 particles cm^{-3}),[93] Eureka and Alert, Canada (with field campaign medians ranging from 100 to 250 particles cm^{-3}),[94] Utqiaġvik, AK (190 particles cm^{-3}, when under Arctic Ocean influence),[27] and the central Arctic Ocean (90−210 particles cm^{-3}).[95] $PM_{2.5}$ BC measurements from the aethalometer showed an average mass concentration of 0.067 μg m^{-3}, which is above the upper threshold (0.05 μg m^{-3}) for clean marine environments.[96] These data support that the "background" periods were more representative of regional oil field conditions than a "clean" Arctic background.

During oil field background periods, the ATOFMS chemically analyzed 17,198 particles between 0.07 and 1.6 μm. The periods were primarily characterized by carbonaceous particles, including OC−amine−sulfate and OC particles, at 54% by number and 58% by mass (Figure 4), because of the regional influence from oil and gas extraction activities. Sulfate and oxidized OC (m/z 43, $C_2H_3O^+$)[60] were internally mixed within 89 and 50%, respectively, of OC−amine−sulfate particles, by number, and 95 and 56% of ECOC particles, by number, respectively. This is consistent with the atmospheric aging within the oil fields. During background periods, average ACSM OA and sulfate mass concentrations were 0.192 and

DOI: 10.1021/acs.est.9b04825
Environ. Sci. Technol. 2020, 54, 92−101

0.014 μg m^{-3}, respectively. OOA averaged 0.16 μg m^{-3} and was 4 times higher than HOA at 0.04 μg m^{-3}.

During background periods, 25% of the 0.07−1.6 μm particle mass was composed of SSA (average 0.20 μg m^{-3}), similar to the plume periods. Considering periods not impacted by plumes, ATOFMS mass concentrations reached a maximum of 5 μg m^{-3} on August 29, due in part to locally produced SSA (Figure 5) during a period of elevated wind speeds (~10 m s^{-1}) (Figure S3). The SSA mass spectra were characterized by Na_xCl_y ions at m/z 81, 83 (Na_2Cl^+), 58, 60 ($NaCl^-$), −93, −95 ($NaCl_2^-$), and −151, −153, −155, −157 ($Na_2Cl_3^-$), as well as chloride at m/z −35, −37 (Cl^-), consistent with the locally produced SSA (Figure S8). The Na_xCl_y ion peaks were more intense in these oil field background SSA particles compared to those of plume period SSA particles (Figure S8), indicative of less atmospheric aging. During oil field background periods, 45 and 16% of the SSA, by number, were internally mixed with nitrate and sulfate, respectively. For these aged SSA, complete chloride displacement had not occurred, similar to previous observations in Utqiaġvik, AK, during oil field air mass influence.[27]

Ultrafine Particle Growth. Ultrafine particle growth was observed from August 24 to 27 during an oil field background period (Figure 6); this period was not included in the previously discussed background averages. Two individual events were observed: August 24 06:00−August 25 20:00 AKDT and August 26 06:00−August 27 00:00. The wind direction did not change during each growth period, suggesting that the observed particle growth was not solely associated with dilution in a shifting plume (Figure S3). The events both had starting diameters of ~20 nm and ending diameters of ~50 nm, with average growth rates of 0.8 and 1.6 nm h^{-1}, respectively (Figure 6). During the growth events, the winds were relatively stagnant at ~4 m s^{-1}, with increased solar radiation and temperature of 132 W m^{-2} and 9 °C, compared to the study averages of 69 W m^{-2} and 3 °C, respectively. Both growth events began during condensation sink[97] minima of ~2 × 10^{-2} s^{-1}, compared to the study average of 2 × 10^{-1} s^{-1}, though the average is skewed high due to brief, but intense, increases in particle number concentrations within plumes (Figure S9). While this condensation sink is orders of magnitude higher than previously observed during particle growth in the clean Arctic (2 × 10^{-3} s^{-1}),[98] stagnant winds combined with elevated oxidants and condensable material from oil field emissions likely contributed to the observed aerosol growth. Condensation sinks of ~2 × 10^{-2} s^{-1} were also observed between September 5 and 10 (Figure S9); however, elevated wind speeds of ~10 m s^{-1} during this period likely hindered particle growth.

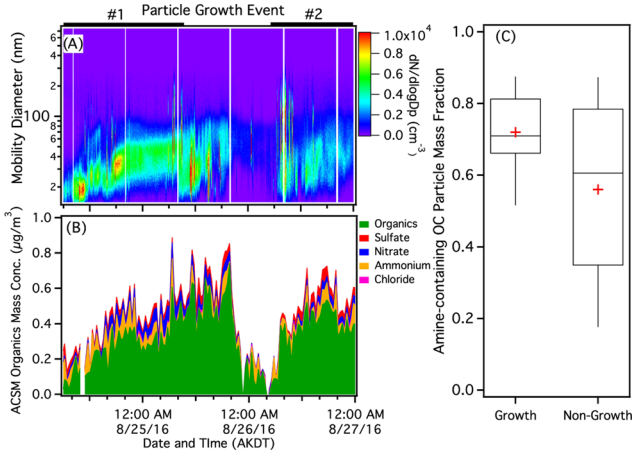

Figure 6. (A) Aerosol number concentration size distributions (14−740 nm, mobility diameter) during two particle growth events that occurred from August 24 06:00 to August 25 20:00 AKDT and August 26 06:00 to August 27 00:00. (B) Mass concentrations of the nonrefractory species measured by ACSM. (C) Mass fractions of amine-containing particles, compared to the sum of all predominately OC particles (OC−amine−sulfate, OC, and biomass burning), for the growth, compared to nongrowth, time periods of the study. The boxes show the 25th, 50th, and 75th percentile values; the whiskers show the 5th and 95th percentile values, with the markers showing average values.

During the two growth events, the mass fraction of amine-containing (OC−amine−sulfate) particles, relative to the predominately organic particles (OC−amine−sulfate, OC, and biomass burning), (0.72) was significantly higher than during the rest of the study (0.56), as shown in Figures 6 and S10. Figure 6B shows that the mass concentration of organics, as measured by ACSM, also increased during the growth events, consistent with the contribution of condensing organics to particle growth. With lower volatility than ammonium sulfate,[99] aminium salts contribute to new particle formation and growth[80,82,100−103] with greater contributions expected at lower temperatures.[104] Previous studies in other locations, including the Canadian Archipelago,[80,103] have also observed increased contributions from submicron amine-containing particles during particle growth events.[105,106] The likely contribution of aminium sulfate salts, originating from the oil fields, to the observed particle growth may explain observations by Kolesar et al.[98] who found particle growth at Utqiaġvik, AK, to preferentially occur in air masses influenced by the North Slope of Alaska oil fields, compared to that of Arctic Ocean air masses.

Atmospheric Implications. Here, we report the first online chemical characterization of atmospheric particles in the North Slope of Alaska (Prudhoe Bay) oil fields, located in the coastal Arctic. The site was constantly influenced by oil field emissions. Combustion plumes originating from nearby oil and gas extraction facilities were characterized. The vast majority of particles within the plumes were ultrafine particles, attributed to combustion. Plumes primarily consisted of soot and organic carbon-containing particles, by both number and mass, and over 90% of these particles, by number, were internally mixed with sulfate, from the oxidation of SO_2 emitted within the oil fields. Soot in the form of EC and ECOC particles primarily originated from diesel combustion, in agreement with recent pan-Arctic carbon isotope measurements.[20] The presence of sulfate and oxidized organic carbon coatings on soot particles may increase absorption[31,107−110] and CCN activity.[17] OC−amine−sulfate particle concentrations were elevated within oil field plumes and are attributed to oil field industrial emissions. Aminium sulfate salts likely contributed to observed particle growth and may explain the preferential aerosol growth observed at Utqiaġvik, AK, during oil-field-influenced air masses, compared to that of clean Arctic Ocean air masses.[98] During both oil field background and plume periods, sea spray aerosol contributed ~20−25% to particle mass concentrations at the coastal site. Compared to the Arctic background, recent cloud measurements showed increased CCN concentrations and lower mean effective radii of cloud droplets above and downwind of the North Slope of Alaska oil fields, leading to

DOI: 10.1021/acs.est.9b04825
Environ. Sci. Technol. 2020, 54, 92−101

suppressed drizzle production and precipitation.[30] With ongoing Arctic development,[8] local combustion emissions are expected to have increasing importance for climate feedbacks and air quality.[21]

■ ASSOCIATED CONTENT

Supporting Information

The Supporting Information is available free of charge at https://pubs.acs.org/doi/10.1021/acs.est.9b04825.

Additional information found in the supplemental include ATOFMS particle-type classification descriptions, size-resolved number and mass concentrations, comparison of ACSM and ATOFMS observations, meteorological parameters, chemically and size-resolved particle number fractions, SSA mass spectral comparison during oil field background and plume periods, and condensation sink plots (PDF)

■ AUTHOR INFORMATION

Corresponding Author

*E-mail: prattka@umich.edu.

ORCID

Qi Zhang: 0000-0002-5203-8778

Kerri A. Pratt: 0000-0003-4707-2290

Author Contributions

#M.J.G. and J.L. contributed equally to this work.

Notes

The authors declare no competing financial interest.

■ ACKNOWLEDGMENTS

This study was supported by the NOAA Climate Program Office Atmospheric Chemistry, Carbon Cycle, and Climate Program through NA14OAR4310149 (University of Michigan) and NA14OAR4310150 (Baylor University). This research was also supported, in part, by the Office of Biological and Environmental Research (BER) of the U.S. DOE as part of the ARM Climate Research Facility, an Office of Science Scientific User Facility (Field campaign 2013−6660). In addition, this research was supported by K.A.P.'s Early-Career Research Fellowship (2000007270) from the Gulf Research Program of the National Academies of Sciences, Engineering, and Medicine; the content is solely the responsibility of the authors and does not necessarily represent the official views of the Gulf Research Program of the National Academies. N.W. and Q.Z. were supported by funding from the DOE Atmospheric System Research Program (DE-SC0014620w). Meteorological and greenhouse gas data were obtained from the ARM Climate Research Facility. DOE ARM, Sandia National Laboratory, AMF3 field operators, and the U.S. Air Force are thanked for logistical assistance at Oliktok Point, AK.

■ REFERENCES

(1) Allison, E. H.; Bassett, H. R. Climate change in the oceans: Human impacts and responses. *Science* **2015**, *350*, 778−782.

(2) Harsem, Ø.; Heen, K.; Rodrigues, J.; Vassdal, T. Oil exploration and sea ice projections in the Arctic. *Polar Rec.* **2015**, *51*, 91−106.

(3) Screen, J. A.; Simmonds, I. The central role of diminishing sea ice in recent Arctic temperature amplification. *Nature* **2010**, *464*, 1334−1337.

(4) IPCC. *Climate Change 2013: The Physical Science Basis. Contribution of working group I to the Fifth Assessment Report of the Intergovernmental Panel on Climate Change*; Cambridge University Press, 2013.

(5) Overland, J. E.; Wang, M. When will the summer Arctic be nearly sea ice free? Geophys. *Res. Lett.* **2013**, *40*, 2097−2101.

(6) Wang, M.; Overland, J. E. Projected future duration of the sea-ice-free season in the Alaskan Arctic. *Prog. Oceanogr.* **2015**, *136*, 50−59.

(7) Swart, N. C.; Fyfe, J. C.; Hawkins, E.; Kay, J. E.; Jahn, A. Influence of internal variability on Arctic sea-ice trends. *Nat. Clim. Change* **2015**, *5*, No. 86.

(8) Gautier, D. L.; Bird, K. J.; Charpentier, R. R.; Grantz, A.; Houseknecht, D. W.; Klett, T. R.; Moore, T. E.; Pitman, J. K.; Schenk, C. J.; Schuenemeyer, J. H. Assessment of undiscovered oil and gas in the Arctic. *Science* **2009**, *324*, 1175−1179.

(9) Mack, A.; Bluemink, E. *State Receives $17.8 million in Oil and Gas Lease Sales*; State of Alaska Department of Natural Resources, 2016.

(10) Peters, G.; Nilssen, T.; Lindholt, L.; Eide, M.; Glomsrød, S.; Eide, L.; Fuglestvedt, J. Future emissions from shipping and petroleum activities in the Arctic. *Atmos. Chem. Phys.* **2011**, *11*, 5305−5320.

(11) Law, K. S.; Stohl, A. Arctic air pollution: Origins and impacts. *Science* **2007**, *315*, 1537−1540.

(12) Pöschl, U. Atmospheric Aerosols: Composition, Transformation, Climate and Health Effects. *Angew. Chem., Int. Ed.* **2005**, *44*, 7520−7540.

(13) Jacobson, M. Z. Climate response of fossil fuel and biofuel soot, accounting for soot's feedback to snow and sea ice albedo and emissivity. *J. Geophys. Res.: Atmos.* **2004**, *109*, No. 4945.

(14) Flanner, M. G. Arctic climate sensitivity to local black carbon. *J. Geophys. Res.: Atmos.* **2013**, *118*, 1840−1851.

(15) Evans, M.; Kholod, N.; Kuklinski, T.; Denysenko, A.; Smith, S. J.; Staniszewski, A.; Hao, W. M.; Liu, L.; Bond, T. C. Black carbon emissions in Russia: A critical review. *Atmos. Environ.* **2017**, *163*, 9−21.

(16) Winiger, P.; Andersson, A.; Eckhardt, S.; Stohl, A.; Semiletov, I. P.; Dudarev, O. V.; Charkin, A.; Shakhova, N.; Klimont, Z.; Heyes, C. Siberian Arctic black carbon sources constrained by model and observation. *Proc. Natl. Acad. Sci. U.S.A.* **2017**, No. 201613401.

(17) Bond, T. C.; Doherty, S. J.; Fahey, D.; Forster, P.; Berntsen, T.; DeAngelo, B.; Flanner, M.; Ghan, S.; Kärcher, B.; Koch, D. Bounding the role of black carbon in the climate system: A scientific assessment. *J. Geophys. Res.: Atmos.* **2013**, *118*, 5380−5552.

(18) Xu, J.-W.; Martin, R. V.; Morrow, A.; Sharma, S.; Huang, L.; Leaitch, W. R.; Burkart, J.; Schulz, H.; Zanatta, M.; Willis, M. D. Source attribution of Arctic black carbon constrained by aircraft and surface measurements. *Atmos. Chem. Phys.* **2017**, *17*, 11971−11989.

(19) Qi, L.; Wang, S. Sources of black carbon in the atmosphere and in snow in the Arctic. *Sci. Total Environ.* **2019**, *691*, 442−454.

(20) Winiger, P.; Barrett, T.; Sheesley, R.; Huang, L.; Sharma, S.; Barrie, L.; Yttri, K. E.; Evangeliou, N.; Eckhardt, S.; Stohl, A. Source apportionment of circum-Arctic atmospheric black carbon from isotopes and modeling. *Sci. Adv.* **2019**, *5*, No. eaau8052.

(21) Schmale, J.; Arnold, S.; Law, K. S.; Thorp, T.; Anenberg, S.; Simpson, W.; Mao, J.; Pratt, K. Local Arctic air pollution: A neglected but serious problem. *Earth's Future* **2018**, *6*, 1385−1412.

(22) Jaffe, D.; Honrath, R.; Furness, D.; Conway, T.; Dlugokencky, E.; Steele, L. A determination of the CH4, NO x and CO2 emissions from the Prudhoe Bay, Alaska oil development. *J. Atmos. Chem.* **1995**, *20*, 213−227.

(23) Brooks, S. B.; Crawford, T. L.; Oechel, W. C. Measurement of carbon dioxide emissions plumes from Prudhoe Bay, Alaska oil fields. *J. Atmos. Chem.* **1997**, *27*, 197−207.

(24) Brock, C. A.; Cozic, J.; Bahreini, R.; Froyd, K. D.; Middlebrook, A. M.; McComiskey, A.; Brioude, J.; Cooper, O.; Stohl, A.; Aikin, K. Characteristics, sources, and transport of aerosols measured in spring 2008 during the aerosol, radiation, and cloud processes affecting Arctic Climate (ARCPAC) Project. *Atmos. Chem. Phys.* **2011**, *11*, 2423−2453.

DOI: 10.1021/acs.est.9b04825
Environ. Sci. Technol. 2020, 54, 92−101

(25) Stohl, A.; Klimont, Z.; Eckhardt, S.; Kupiainen, K.; Shevchenko, V.; Kopeikin, V.; Novigatsky, A. Black carbon in the Arctic: the underestimated role of gas flaring and residential combustion emissions. *Atmos. Chem. Phys.* **2013**, *13*, 8833−8855.
(26) Roiger, A.; Thomas, J.-L.; Schlager, H.; Law, K. S.; Kim, J.; Schäfler, A.; Weinzierl, B.; Dahlkötter, F.; Krisch, I.; Marelle, L. Quantifying emerging local anthropogenic emissions in the Arctic region: The ACCESS aircraft campaign experiment. *B. Am. Meteorol. Soc.* **2015**, *96*, 441−460.
(27) Gunsch, M. J.; Kirpes, R. M.; Kolesar, K. R.; Barrett, T. E.; China, S.; Sheesley, R. J.; Laskin, A.; Wiedensohler, A.; Tuch, T.; Pratt, K. A. Contributions of transported Prudhoe Bay oil field emissions to the aerosol population in Utqiaġvik, Alaska. *Atmos. Chem. Phys.* **2017**, *17*, 10879−10892.
(28) Maahn, M.; de Boer, G.; Creamean, J.; Feingold, G.; McFarquhar, G. M.; Wu, W.; Mei, F. The observed influence of local anthropogenic pollution on northern Alaskan cloud properties. *Atmos. Chem. Phys.* **2017**, *17*, No. 2017.
(29) Creamean, J. M.; Maahn, M.; de Boer, G.; McComiskey, A.; Sedlacek, A. J.; Feng, Y. The influence of local oil exploration and regional wildfires on summer 2015 aerosol over the North Slope of Alaska. *Atmos. Chem. Phys.* **2018**, *18*, 555−570.
(30) Maahn, M.; de Boer, G.; Creamean, J.; Feingold, G.; McFarquhar, G. M.; Wu, W.; Mei, F. The observed influence of local anthropogenic pollution on northern Alaskan cloud properties. *Atmos. Chem. Phys.* **2017**, *17*, 14709−14726.
(31) Moffet, R. C.; Prather, K. A. In-situ measurements of the mixing state and optical properties of soot with implications for radiative forcing estimates. *Proc. Natl. Acad. Sci.* **2009**, *106*, 11872−11877.
(32) Sharma, S.; Ishizawa, M.; Chan, D.; Lavoué, D.; Andrews, E.; Eleftheriadis, K.; Maksyutov, S. 16-year simulation of Arctic black carbon: Transport, source contribution, and sensitivity analysis on deposition. *J. Geophys. Res.: Atmos.* **2013**, *118*, 943−964.
(33) Riemer, N.; Ault, A. P.; West, M.; Craig, R. L.; Curtis, J. H. Aerosol Mixing State: Measurements, Modeling, and Impacts. *Rev. Geophys.* **2019**, *57*, DOI: 10.1029/2018rg000615.
(34) Pratt, K. A.; Prather, K. A. Real-time, single-particle volatility, size, and chemical composition measurements of aged urban aerosols. *Environ. Sci. Technol.* **2009**, *43*, 8276−8282.
(35) Ault, A. P.; Moore, M. J.; Furutani, H.; Prather, K. A. Impact of emissions from the Los Angeles port region on San Diego air quality during regional transport events. *Environ. Sci. Technol.* **2009**, *43*, 3500−3506.
(36) Gross, D. S.; Barron, A. R.; Sukovich, E. M.; Warren, B. S.; Jarvis, J. C.; Suess, D. T.; Prather, K. A. Stability of single particle tracers for differentiating between heavy-and light-duty vehicle emissions. *Atmos. Environ.* **2005**, *39*, 2889−2901.
(37) Toner, S. M.; Shields, L. G.; Sodeman, D. A.; Prather, K. A. Using mass spectral source signatures to apportion exhaust particles from gasoline and diesel powered vehicles in a freeway study using UF-ATOFMS. *Atmos. Environ.* **2008**, *42*, 568−581.
(38) Vogt, R.; Kirchner, U.; Scheer, V.; Hinz, K.; Trimborn, A.; Spengler, B. Identification of diesel exhaust particles at an Autobahn, urban and rural location using single-particle mass spectrometry. *J. Aerosol. Sci.* **2003**, *34*, 319−337.
(39) Healy, R. M.; O'Connor, I. P.; Hellebust, S.; Allanic, A.; Sodeau, J. R.; Wenger, J. C. Characterisation of single particles from in-port ship emissions. *Atmos. Environ.* **2009**, *43*, 6408−6414.
(40) Ault, A. P.; Gaston, C. J.; Wang, Y.; Dominguez, G.; Thiemens, M. H.; Prather, K. A. Characterization of the single particle mixing state of individual ship plume events measured at the port of Los Angeles. *Environ. Sci. Technol.* **2010**, *44*, 1954−1961.
(41) Guazzotti, S.; Suess, D.; Coffee, K.; Quinn, P.; Bates, T.; Wisthaler, A.; Hansel, A.; Ball, W.; Dickerson, R.; Neusüß, C. Characterization of carbonaceous aerosols outflow from India and Arabia: Biomass/biofuel burning and fossil fuel combustion. *J. Geophys. Res.: Atmos.* **2003**, *108*, No. 3277.
(42) Yang, J.; Ma, S.; Gao, B.; Li, X.; Zhang, Y.; Cai, J.; Li, M.; Yao, La.; Huang, B.; Zheng, M. , Single particle mass spectral signatures from vehicle exhaust particles and the source apportionment of on-line PM 2.5 by single particle aerosol mass spectrometry. *Sci. Total Environ.* **2017**, *593*, 310−318.
(43) Pratt, K. A.; Mayer, J. E.; Holecek, J. C.; Moffet, R. C.; Sanchez, R. O.; Rebotier, T. P.; Furutani, H.; Gonin, M.; Fuhrer, K.; Su, Y. Development and characterization of an aircraft aerosol time-of-flight mass spectrometer. *Anal. Chem.* **2009**, *81*, 1792−1800.
(44) Ng, N. L.; Herndon, S. C.; Trimborn, A.; Canagaratna, M. R.; Croteau, P. L.; Onasch, T. B.; Sueper, D.; Worsnop, D. R.; Zhang, Q.; Sun, Y. L.; Jayne, J. T. An Aerosol Chemical Speciation Monitor (ACSM) for Routine Monitoring of the Composition and Mass Concentrations of Ambient Aerosol. *Aerosol Sci. Technol.* **2011**, *45*, 780−794.
(45) Fröhlich, R.; Cubison, M.; Slowik, J.; Bukowiecki, N.; Prévôt, A.; Baltensperger, U.; Schneider, J.; Kimmel, J.; Gonin, M.; Rohner, U. The ToF-ACSM: a portable aerosol chemical speciation monitor with TOFMS detection. *Atmos. Meas. Tech.* **2013**, *6*, 3225−3241.
(46) Andreas, A.; Habte, A.; Reda, I.; Dooraghi, M.; Kutchenreiter, M.; Sengupta, M.; Morris, V.; Xie, Y.Atmospheric Radiation Measurement (ARM) Climate Research Facility. 2013, updated hourly. Sky Radiometers on Stand for Downwelling Radiation (SKYRAD60S). 2016-08-01 to 2016-09-29, ARM Mobile Facility (OLI) Olikiok Point, Alaska; AMF3 (M1). (Data set accessed 2017-09-20 at http://dx.doi.org/10.5439/1025281.).
(47) Holdridge, D.; Kyrouac, J.Atmospheric Radiation Measurement (ARM) Climate Research Facility. 1993, updated hourly. Surface Meteorological Instrumentation (MET). 2016-08-20 to 2016-09-19, 70.495 N 149.886 W: ARM Mobile Facility (OLI) Olikiok Point, Alaska; AMF3 (M1). (Data set accessed 2016-10-17 at http://dx.doi.org/10.5439/1025220.).
(48) Behrens, B.; Salwen, C.; Hageman, D.; Uin, J.; Smith, S.; Koontz, A.; Jefferson, A.; Sedlacek, A.; Kuang, C.; Senum, G.; Dubey, M.; Springston, S.; Watson, T.Atmospheric Radiation Measurement (ARM) Climate Research Facility. 2012, updated hourly. Trace gas concentrations (AOSCO). 2016-08-05 to 2016-09-18, 70.495 N 149.886 W: ARM Mobile Facility (OLI) Olikiok Point, Alaska; AMF3 (M1). (Data set accessed 2017-01-04 at http://dx.doi.org/10.5439/1250819).
(49) Paatero, P.; Tapper, U. Positive Matrix Factorization: A Non-Negative Factor Model with Optimal Utilization of Error Estimates of Data Values. *Environmetrics* **1994**, *5*, 111−126.
(50) Ulbrich, I. M.; Canagaratna, M. R.; Zhang, Q.; Worsnop, D. R.; Jimenez, J. L. Interpretation of organic components from Positive Matrix Factorization of aerosol mass spectrometric data. *Atmos. Chem. Phys.* **2009**, *9*, 2891−2918.
(51) Zhang, Q.; Jimenez, J. L.; Canagaratna, M. R.; Ulbrich, I. M.; Ng, N. L.; Worsnop, D. R.; Sun, Y. L. Understanding atmospheric organic aerosols via factor analysis of aerosol mass spectrometry: a review. *Anal. Bioanal. Chem.* **2011**, *401*, 3045−3067.
(52) Ng, N. L.; Canagaratna, M. R.; Jimenez, J. L.; Zhang, Q.; Ulbrich, I. M.; Worsnop, D. R. Real-Time Methods for Estimating Organic Component Mass Concentrations from Aerosol Mass Spectrometer Data. *Environ. Sci. Technol.* **2011**, *45*, 910−916.
(53) Schmid, O.; Artaxo, P.; Arnott, W.; Chand, D.; Gatti, L. V.; Frank, G.; Hoffer, A.; Schnaiter, M.; Andreae, M. Spectral light absorption by ambient aerosols influenced by biomass burning in the Amazon Basin. I: Comparison and field calibration of absorption measurement techniques. *Atmos. Chem. Phys.* **2006**, *6*, 3443−3462.
(54) Khlystov, A.; Stanier, C.; Pandis, S. An algorithm for combining electrical mobility and aerodynamic size distributions data when measuring ambient aerosol. *Aerosol. Sci. Technol.* **2004**, *38*, 229−238.
(55) Neubauer, K. R.; Johnston, M. V.; Wexler, A. S. On-line analysis of aqueous aerosols by laser desorption ionization. *Int. J. Mass. Spectrom.* **1997**, *163*, 29−37.
(56) Spencer, M.; Holecek, J.; Corrigan, C.; Ramanathan, V.; Prather, K. Size-resolved chemical composition of aerosol particles

DOI: 10.1021/acs.est.9b04825
Environ. Sci. Technol. 2020, 54, 92−101

during a monsoonal transition period over the Indian Ocean. *J. Geophys. Res.: Atmos.* **2008**, *113*, 305.
(57) Sultana, C. M.; Cornwell, G. C.; Rodriguez, P.; Prather, K. A. FATES: a flexible analysis toolkit for the exploration of single-particle mass spectrometer data. *Atmos. Meas. Tech.* **2017**, *10*, 1323−1334.
(58) Song, X.-H.; Hopke, P. K.; Fergenson, D. P.; Prather, K. A. Classification of single particles analyzed by ATOFMS using an artificial neural network, ART-2A. *Anal. Chem.* **1999**, *71*, 860−865.
(59) Qin, X.; Bhave, P. V.; Prather, K. A. Comparison of two methods for obtaining quantitative mass concentrations from aerosol time-of-flight mass spectrometry measurements. *Anal. Chem.* **2006**, *78*, 6169−6178.
(60) Qin, X.; Pratt, K. A.; Shields, L. G.; Toner, S. M.; Prather, K. A. Seasonal comparisons of single-particle chemical mixing state in Riverside, CA. *Atmos. Environ.* **2012**, *59*, 587−596.
(61) Spencer, M. T.; Shields, L. G.; Prather, K. A. Simultaneous measurement of the effective density and chemical composition of ambient aerosol particles. *Environ. Sci. Technol.* **2007**, *41*, 1303−1309.
(62) Moffet, R. C.; Qin, X.; Rebotier, T.; Furutani, H.; Prather, K. A. Chemically segregated optical and microphysical properties of ambient aerosols measured in a single-particle mass spectrometer. *J. Geophys. Res.: Atmos.* **2008**, *113*, No. D12213.
(63) Zelenyuk, A.; Cai, Y.; Imre, D. From agglomerates of spheres to irregularly shaped particles: Determination of dynamic shape factors from measurements of mobility and vacuum aerodynamic diameters. *Aerosol Sci. Technol.* **2006**, *40*, 197−217.
(64) Zelenyuk, A.; Cai, Y.; Chieffo, L.; Imre, D. High precision density measurements of single particles: The density of metastable phases. *Aerosol Sci. Technol.* **2005**, *39*, 972−986.
(65) Moffet, R. C.; Prather, K. A. Extending ATOFMS measurements to include refractive index and density. *Anal. Chem.* **2005**, *77*, 6535−6541.
(66) Vaden, T. D.; Song, C.; Zaveri, R. A.; Imre, D.; Zelenyuk, A. Morphology of mixed primary and secondary organic particles and the adsorption of spectator organic gases during aerosol formation. *Proc. Natl. Acad. Sci. U.S.A.* **2010**, *107*, 6658−6663.
(67) Zelenyuk, A.; Yang, J.; Song, C.; Zaveri, R. A.; Imre, D. "Depth-profiling" and quantitative characterization of the size, composition, shape, density, and morphology of fine particles with SPLAT, a single-particle mass spectrometer. *J. Phys. Chem. A* **2008**, *112*, 669−677.
(68) Birch, M.; Cary, R. Elemental carbon-based method for monitoring occupational exposures to particulate diesel exhaust. *Aerosol Sci. Technol.* **1996**, *25*, 221−241.
(69) Yoon, S.; Fairley, D.; Barrett, T. E.; Sheesley, R. J. Biomass and fossil fuel combustion contributions to elemental carbon across the San Francisco Bay Area. *Atmos. Environ.* **2018**, *195*, 229−242.
(70) Prather, K. A.; Bertram, T. H.; Grassian, V. H.; Deane, G. B.; Stokes, M. D.; DeMott, P. J.; Aluwihare, L. I.; Palenik, B. P.; Azam, F.; Seinfeld, J. H. Bringing the ocean into the laboratory to probe the chemical complexity of sea spray aerosol. *Proc. Natl. Acad. Sci. U.S.A.* **2013**, *110*, 7550−7555.
(71) Quinn, P.; Miller, T.; Bates, T.; Ogren, J.; Andrews, E.; Shaw, G. A 3-year record of simultaneously measured aerosol chemical and optical properties at Barrow, Alaska. *J. Geophys. Res.: Atmos.* **2002**, *107*, 8−15.
(72) Spencer, M. T.; Shields, L. G.; Sodeman, D. A.; Toner, S. M.; Prather, K. A. Comparison of oil and fuel particle chemical signatures with particle emissions from heavy and light duty vehicles. *Atmos. Environ.* **2006**, *40*, 5224−5235.
(73) Silva, P. J.; Prather, K. A. Interpretation of mass spectra from organic compounds in aerosol time-of-flight mass spectrometry. *Anal. Chem.* **2000**, *72*, 3553−3562.
(74) Angelino, S.; Suess, D. T.; Prather, K. A. Formation of aerosol particles from reactions of secondary and tertiary alkylamines: Characterization by aerosol time-of-flight mass spectrometry. *Environ. Sci. Technol.* **2001**, *35*, 3130−3138.
(75) Pratt, K. A.; Hatch, L. E.; Prather, K. A. Seasonal volatility dependence of ambient particle phase amines. *Environ. Sci. Technol.* **2009**, *43*, 5276−5281.
(76) Denkenberger, K. A.; Moffet, R. C.; Holecek, J. C.; Rebotier, T. P.; Prather, K. A. Real-time, single-particle measurements of oligomers in aged ambient aerosol particles. *Environ. Sci. Technol.* **2007**, *41*, 5439−5446.
(77) Huang, Y.; Chen, H.; Wang, L.; Yang, X.; Chen, J. Single particle analysis of amines in ambient aerosol in Shanghai. *Environ. Chem.* **2012**, *9*, 202−210.
(78) Ge, X.; Wexler, A. S.; Clegg, S. L. Atmospheric amines−Part I. A review. *Atmos. Environ.* **2011**, *45*, 524−546.
(79) Dall'Osto, M.; Drewnick, F.; Fisher, R.; Harrison, R. M. Real-time measurements of nonmetallic fine particulate matter adjacent to a major integrated steelworks. *Aerosol Sci. Technol.* **2012**, *46*, 639−653.
(80) Willis, M. D.; Köllner, F.; Burkart, J.; Bozem, H.; Thomas, J. L.; Schneider, J.; Aliabadi, A. A.; Hoor, P. M.; Schulz, H.; Herber, A. B. Evidence for marine biogenic influence on summertime Arctic aerosol. *Geophys. Res. Lett.* **2017**, *44*, 6460−6470.
(81) Köllner, F.; Schneider, J.; Willis, M. D.; Klimach, T.; Helleis, F.; Bozem, H.; Kunkel, D.; Hoor, P.; Burkart, J.; Leaitch, W. R.; Aliabadi, A. A.; Abbatt, J. P. D.; Herber, A. B.; Borrmann, S. Particulate trimethylamine in the summertime Canadian high Arctic lower troposphere. *Atmos. Chem. Phys.* **2017**, *2017*, 13747−13766.
(82) Dall'Osto, M.; Airs, R. L.; Beale, R.; Cree, C.; Fitzsimons, M. F.; Beddows, D.; Harrison, R. M.; Ceburnis, D.; O'Dowd, C.; Rinaldi, M. Simultaneous detection of alkylamines in the surface ocean and atmosphere of the Antarctic sympagic environment. *ACS Earth Space Chem.* **2019**, *3*, 854−862.
(83) Dall'Osto, M.; Ovadnevaite, J.; Paglione, M.; Beddows, D. C. S.; Ceburnis, D.; Cree, C.; Cortes, P.; Zamanillo, M.; Nunes, S. O.; Perez, G. L.; Ortega-Retuerta, E.; Emelianov, M.; Vaque, D.; Marrase, C.; Estrada, M.; Sala, M. M.; Vidal, M.; Fitzsimons, M. F.; Beale, R.; Airs, R.; Rinaldi, M.; Decesari, S.; Facchini, M. C.; Harrison, R. M.; O'Dowd, C.; Simo, R. Antarctic sea ice region as a source of biogenic organic nitrogen in aerosols. *Sci. Rep.* **2017**, No. 6047.
(84) Toner, S. M.; Sodeman, D. A.; Prather, K. A. Single particle characterization of ultrafine and accumulation mode particles from heavy duty diesel vehicles using aerosol time-of-flight mass spectrometry. *Environ. Sci. Technol.* **2006**, *40*, 3912−3921.
(85) Spencer, M. T.; Prather, K. A. Using ATOFMS to determine OC/EC mass fractions in particles. *Aerosol Sci. Technol.* **2006**, *40*, 585−594.
(86) Buonanno, G.; Dell'Isola, M.; Stabile, L.; Viola, A. Uncertainty Budget of the SMPS−APS System in the Measurement of PM1, PM2.5, and PM10. *Aerosol Sci. Technol.* **2009**, *43*, 1130−1141.
(87) Budisulistiorini, S.; Canagaratna, M.; Croteau, P.; Baumann, K.; Edgerton, E.; Kollman, M.; Ng, N.; Verma, V.; Shaw, S.; Knipping, E. Intercomparison of an Aerosol Chemical Speciation Monitor (ACSM) with ambient fine aerosol measurements in downtown Atlanta, Georgia. *Atmos. Meas. Tech.* **2014**, *7*, 1929−1941.
(88) Reid, J.; Koppmann, R.; Eck, T.; Eleuterio, D. A review of biomass burning emissions part II: intensive physical properties of biomass burning particles. *Atmos. Chem. Phys.* **2005**, *5*, 799−825.
(89) Wallace, J. M.; Hobbs, P. V. *Atmospheric Science: An Introductory Survey*; Academic Press, 2006; Vol. *92*.
(90) Ault, A. P.; Guasco, T. L.; Baltrusaitis, J.; Ryder, O. S.; Trueblood, J. V.; Collins, D. B.; Ruppel, M. J.; Cuadra-Rodriguez, L. A.; Prather, K. A.; Grassian, V. H. Heterogeneous reactivity of nitric acid with nascent sea spray aerosol: Large differences observed between and within individual particles. *J. Phys. Chem. Lett.* **2014**, *5*, 2493−2500.
(91) Gard, E. E.; Kleeman, M. J.; Gross, D. S.; Hughes, L. S.; Allen, J. O.; Morrical, B. D.; Fergenson, D. P.; Dienes, T.; Gälli, M. E.; Johnson, R. J. Direct observation of heterogeneous chemistry in the atmosphere. *Science* **1998**, *279*, 1184−1187.
(92) Nguyen, Q. T.; Glasius, M.; Sørensen, L. L.; Jensen, B.; Skov, H.; Birmili, W.; Wiedensohler, A.; Kristensson, A.; Nøjgaard, J. K.; Massling, A. Seasonal variation of atmospheric particle number concentrations, new particle formation and atmospheric oxidation

DOI: 10.1021/acs.est.9b04825
Environ. Sci. Technol. 2020, 54, 92−101

capacity at the high Arctic site Villum Research Station, Station Nord. *Atmos. Chem. Phys.* **2016**, *16*, 11319−11336.
(93) Asmi, E.; Kondratyev, V.; Brus, D.; Laurila, T.; Lihavainen, H.; Backman, J.; Vakkari, V.; Aurela, M.; Hatakka, J.; Viisanen, Y. Aerosol size distribution seasonal characteristics measured in Tiksi, Russian Arctic. *Atmos. Chem. Phys.* **2016**, *16*, 1271−1287.
(94) Tremblay, S.; Picard, J.-C.; Bachelder, J. O.; Lutsch, E.; Strong, K.; Fogal, P.; Leaitch, W. R.; Sharma, S.; Kolonjari, F.; Cox, C. J. Characterization of aerosol growth events over Ellesmere Island during the summers of 2015 and 2016. *Atmos. Chem. Phys.* **2019**, *19*, 5589−5604.
(95) Heintzenberg, J.; Leck, C.; Tunved, P. Potential source regions and processes of aerosol in the summer Arctic. *Atmos. Chem. Phys* **2015**, *15*, 6487−6502.
(96) Gantt, B.; Meskhidze, N. The physical and chemical characteristics of marine primary organic aerosol: a review. *Atmos. Chem. Phys.* **2013**, *13*, 3979−3996.
(97) Dal Maso, M.; Kulmala, M.; Lehtinen, K.; Mäkelä, J.; Aalto, P.; O'Dowd, C. Condensation and coagulation sinks and formation of nucleation mode particles in coastal and boreal forest boundary layers. *J. Geophys. Res.: Atmos.* **2002**, *107*, No. 8097.
(98) Kolesar, K. R.; Cellini, J.; Peterson, P. K.; Jefferson, A.; Tuch, T.; Birmili, W.; Wiedensohler, A.; Pratt, K. A. Effect of Prudhoe Bay emissions on atmospheric aerosol growth events observed in Utqiaġvik (Barrow), Alaska. *Atmos. Environ.* **2017**, *152*, 146−155.
(99) Lavi, A.; Bluvshtein, N.; Segre, E.; Segev, L.; Flores, M.; Rudich, Y. Thermochemical, cloud condensation nucleation ability, and optical properties of alkyl aminium sulfate aerosols. *J. Phys. Chem. C* **2013**, *117*, 22412−22421.
(100) Smith, J. N.; Barsanti, K. C.; Friedli, H. R.; Ehn, M.; Kulmala, M.; Collins, D. R.; Scheckman, J. H.; Williams, B. J.; McMurry, P. H. Observations of aminium salts in atmospheric nanoparticles and possible climatic implications. *Proc. Natl. Acad. Sci. U.S.A.* **2010**, *107*, 6634−6639.
(101) Almeida, J.; Schobesberger, S.; Kürten, A.; Ortega, I. K.; Kupiainen-Määttä, O.; Praplan, A. P.; Adamov, A.; Amorim, A.; Bianchi, F.; Breitenlechner, M. Molecular understanding of sulphuric acid-amine particle nucleation in the atmosphere. *Nature* **2013**, *502*, 359−363.
(102) Smith, J.; Dunn, M.; VanReken, T.; Iida, K.; Stolzenburg, M.; McMurry, P.; Huey, L. Chemical composition of atmospheric nanoparticles formed from nucleation in Tecamac, Mexico: Evidence for an important role for organic species in nanoparticle growth. *Geophys. Res. Lett.* **2008**, *35*, No. 32523.
(103) Dall'Osto, M.; Ceburnis, D.; Monahan, C.; Worsnop, D. R.; Bialek, J.; Kulmala, M.; Kurten, T.; Ehn, M.; Wenger, J.; Sodeau, J.; Healy, R.; O'Dowd, C. Nitrogenated and aliphatic organic vapors as possible drivers for marine secondary organic aerosol growth. *J. Geophys. Res.: Atmos.* **2012**, *117*, No. 17522.
(104) Chen, H.; Finlayson-Pitts, B. J. New Particle Formation from Methanesulfonic Acid and Amines/Ammonia as a Function of Temperature. *Environ. Sci. Technol.* **2016**, *51*, 243−252.
(105) Tao, Y.; Ye, X.; Jiang, S.; Yang, X.; Chen, J.; Xie, Y.; Wang, R. Effects of amines on particle growth observed in new particle formation events. *J. Geophys. Res.: Atmos.* **2016**, *121*, 324−335.
(106) Creamean, J. M.; Ault, A. P.; Ten Hoeve, J. E.; Jacobson, M. Z.; Roberts, G. C.; Prather, K. A. Measurements of Aerosol Chemistry during New Particle Formation Events at a Remote Rural Mountain Site. *Environ. Sci. Technol.* **2011**, *45*, 8208−8216.
(107) Jacobson, M. Z. Strong radiative heating due to the mixing state of black carbon in atmospheric aerosols. *Nature* **2001**, *409*, 695−697.
(108) Chung, S. H.; Seinfeld, J. H. Climate response of direct radiative forcing of anthropogenic black carbon. *J. Geophys. Res.: Atmos.* **2005**, *110*, 102.
(109) Knox, A.; Evans, G.; Brook, J.; Yao, X.; Jeong, C.-H.; Godri, K.; Sabaliauskas, K.; Slowik, J. Mass absorption cross-section of ambient black carbon aerosol in relation to chemical age. *Aerosol. Sci. Technol.* **2009**, *43*, 522−532.
(110) Liu, S.; Aiken, A. C.; Gorkowski, K.; Dubey, M. K.; Cappa, C. D.; Williams, L. R.; Herndon, S. C.; Massoli, P.; Fortner, E. C.; Chhabra, P. S. Enhanced light absorption by mixed source black and brown carbon particles in UK winter. *Nat. Commun.* **2015**, *6*, No. 8435.

DOI: 10.1021/acs.est.9b04825
Environ. Sci. Technol. 2020, 54, 92−101